A Scheme for the Power Control in a DFIG Connected to a DC-Bus via a Diode Rectifier

Matteo F. Iacchetti, *Member IEEE*, Gil D. Marques, *Senior Member IEEE*, Roberto Perini, *Member IEEE*

***Abstract*— This paper deals with a new conversion topology for DFIGs suitable for wind energy conversion systems integrated in micro-grids. It consists of a DFIG which is fed by a PWM converter on the rotor and with the stator connected to a dc grid through a diode rectifier. In this configuration, the stator diode rectifier and the rotor-side inverter share the same dc-bus, so that the conventional grid-side inverter is avoided. Since only a diode rectifier designed for the full power and a reduced power inverter are required, this layout allows a cheap and effective integration of the DFIG with other generating and storage systems connected to the same dc-bus. A simple control technique suitable to regulate the power delivered to the dc grid is proposed. The scheme is based on the regulation of the amplitude of a suited fraction of the rotor flux linkage: the optimal value of this fraction is theoretically deduced in order to minimize the DFIG derating due to the current harmonics. The effectiveness of the proposed control is proven by simulations and experimental tests.**

***Index Terms*— Doubly-fed induction machine. Dc-link, Rectifier, Field oriented control, Dc grid.**

NOMENCLATURE

a	factor for the equivalent circuit transformation
A_{sn} , A_{rn}	stator, rotor apparent power
$\bar{e}_s$, $\bar{e}_r$	stator, rotor EMF space vector
$\bar{i}_s$, $\bar{i}_r$	stator, rotor current space vector
k	ratio A_{rn}/A_{sn}
R_s , R_r	stator, rotor resistance
L_s , M, L_r	stator, magnetizing, rotor inductance
m	ratio V_{DC} / peak phase voltage due to $\bar{\psi}_x$
n_{12}	stator-rotor turn ratio
t_e , T_e	instantaneous, average electromagnetic torque
$\bar{v}_s$, $\bar{v}_r$	stator, rotor voltage space vector
V_{DC}	DC-bus voltage
θ_s , θ_r	d-axis position with respect to the stator, rotor
σ	leakage factor $1 - M^2/(L_S L_r)$
$\bar{\psi}_s$, $\bar{\psi}_r$	stator, rotor flux linkage space vector
$\bar{\psi}_x$	fraction of flux linkage space vector
ω_b	rated angular frequency
ω_s, ω_r, ω_m	stator frequency, slip speed, rotor speed (p.u.)

Superscripts

$\bar{x}$	complex quantity
*	set point value

Subscripts

n	rated value
s , r	stator, rotor
α , β	stationary axes
d , q	oriented frame axes

Manuscript received July 26, 2014; revised November 15, 2013 and January 30, 2014; accepted April 9, 2014.

This work was supported by national funds through FCT Fundação para a Ciência e a Tecnologia, under project PEst-OE/EEI/LA0021/2013. Paper no. TPEL-Reg-2013-07-1064

M. F. Iacchetti and R. Perini are with the Dipartimento di Energia, Politecnico di Milano, Dipartimento di Energia via Lambruschini 4, 20156 Milan, Italy (e-mail: matteo.iacchetti@polimi.it, roberto.perini@polimi.it)

G. D. Marques is with the INESC-ID, Instituto Superior Ténico (IST), Universidade de Lisboa, Av. Rovisco Pais, no 1, 1049-001 Lisbon, Portugal (e-mail: gil.marques@tecnico.ulisboa.pt).

I. INTRODUCTION

DOUBLY FED Induction Generators (DFIGs) have been extensively used in wind energy conversion [1], because the rating power of the back-to-back converter in per-unit roughly equals the magnitude of the maximum slip, which typically does not exceed 0.33. In conventional systems, the DFIG is connected to an ac grid: the rotor side converter controls the active and reactive stator power whereas the grid side converter is synchronized with the grid [2]. In the stand-alone operation, the DFIG has to control both voltage and frequency to the rated value. Field oriented control (FOC) based on rotor current loops [2] and direct power control [3] are the most used regulation techniques for DFIGs. Some methods aimed to replace the encoder by a rotor position estimator in the FOC have been also developed, for instance, by using model reference adaptive systems or phase-looked-loop techniques [4]-[10].

In order to meet the requirements of the grid codes, the control systems of DFIGs are becoming more and more advanced. One of the main issues in the control of grid connected DFIGs is to tackle the effects of dips in the stator voltage, which produce oscillations of the stator flux linkage and rotor over-voltages [11]-[12]. An adequate low-voltage ride-through capability [13]-[15] during faults in the ac grid must be guaranteed: in [13] an additional grid series converter is used to mitigate the effect of grid voltage changes on the stator voltage, whereas in [14] a dynamic programming power control is considered. Also the unbalance in the grid voltage

has a detrimental impact on the DFIG, due to unequal heating of the stator and rotor windings, and to the oscillations in the dc-bus voltage of the back-to-back converter. In [16], the additional grid series converter proposed in [13] is controlled to compensate for the grid voltage unbalance, whereas Yao *et al.* [17] describe a control of the capacitor current, aimed to eliminate the fluctuations in the dc-bus voltage. Similarly to the unbalance, also the distortion in the grid voltages produces power fluctuations and torque ripple, and increases joule losses in the windings [18]-[21]. Such effects are prominent also in stand-alone DFIGs which feed non-linear loads [4], [22]. Proportional integral (PI) controllers in multiple frames can be used in order to kill the harmonic voltage components in stand-alone DFIGs [22]. Resonant controllers are used in [19]-[20], where the harmonic command currents are chosen according to the desired control target: for instance, either the reduction of the oscillations in the torque or in the stator active and reactive power, or the harmonic reduction in the stator currents. In [21], the 5^{th} and 7^{th} harmonics of the stator current are suppressed by a resonant controller which acts on the rotor current loops.

In spite of the noticeable attention paid to DFIGs connected to ac grids or stand alone ac loads, only few studies [23]-[24] consider the connection of a DFIG to a dc-bus or to a dc grid. This layout is interesting for distributed generation systems [25]-[26] and dc micro-grids [27]-[28], where wind turbines, solar panels, bio-fuel, as well as storage systems could be effectively integrated by means of a common dc-bus. A dc input is also suitable to feed the dc-ac converter and the medium frequency boost transformer in high voltage dc transmission lines [29]-[30].

The simplest way to connect an ac generator to a dc-bus is through a diode rectifier. Differently from permanent magnet synchronous generators, DFIGs can be effectively regulated by controlling the rotor currents through a reduced-size converter, so that a high performance control can be achieved even if the stator is connected to an uncontrolled rectifier. Moreover, a generator connected to a constant voltage dc link by a diode rectifier experiences an almost constant fundamental electromotive force (EMF), which implies an almost constant flux-frequency product. In this case, DFIGs are appropriate, because they can regulate the stator frequency independently of the speed and can work with an almost constant flux in the whole range of the speed. By contrast, in a variable-excitation synchronous generator (VESG), the flux would considerably increase at low speed, and the magnetic circuit should be over-sized or a full power dc-dc converter should be used [31].

The connection of a DFIG to a dc-bus by a diode rectifier has been proposed in [23]: however this system still involves a back-to-back converter, and the grid-side converter is controlled as an active filter in order to obtain sinusoidal stator currents in the DFIG. In [24], a layout based only on a diode rectifier and a single reduced-power PWM converter has been suggested: the stator of the DFIG is connected to a dc-bus through an uncontrolled rectifier, such a dc bus also feeds the rotor side inverter. This way, the grid-side inverter is avoided, resulting in a significant volume saving and cost reduction. Controlling a DFIG connected to a dc grid through a diode rectifier simultaneously involves two issues which belong to different traditional configurations. In fact, as in stand-alone systems, the stator frequency is not imposed by an ac grid and must be controlled near the rated frequency of the machine, in order to exploit the rated apparent power and to limit the level of the flux. On the other hand, if the dc bus is regulated by other devices, the DFIG torque should be controlled in order to operate around the maximum power point of the prime mover, as in ac-grid connected DFIGs.

In [24], a frequency control based on the adjustment of the d-axis rotor current in a frame aligned to the stator flux linkage has been discussed. However, only preliminary results have been reported in [24], no discussion of the effect of the current harmonics on the derating of the DFIG has been provided.

This paper proposes a control technique for the dc power based on the regulation of the amplitude of a suitable fraction of the rotor flux linkage space vector, which takes into account only a partial rotor leakage contribution. With respect to the orientation of the control frame along the stator or the rotor flux space vector (as usual in DFIG or squirrel cage machines respectively), the method proposed in this paper allows an optimal tuning of the inductance involved in the diode commutations, in order to maximize the transferred power-per-ampere. This issue is investigated in this paper by using a steady state model of the diode rectifier. Moreover, the paper discusses the choice of the most proper DFIG rated stator voltage for the connection to a dc bus with a given voltage as well as some implementation issues.

The structure of the paper is as follows. Section II presents the conversion topology, whereas section III summarizes the DFIG dynamic model. Section IV introduces the control scheme and discusses the optimal value of the fraction of the rotor flux linkage to be controlled as well as the optimal values of the DFIG rated stator voltage and turn-ratio. Section V illustrates the implementation of the control scheme. Section VI shows some simulation results. Finally, Section VII reports some experimental results obtained by a laboratory setup.

II. Conversion Topology

The conversion topology is shown in Fig. 1: the diode rectifier and the rotor side inverter share the same dc-bus. The rectifier here considered is an ordinary six-pulse diode bridge. In this work, the dc voltage V_{dc} is considered constant: this is reasonable if we assume that V_{dc} is controlled by other devices (for instance storage systems) connected to the dc grid.

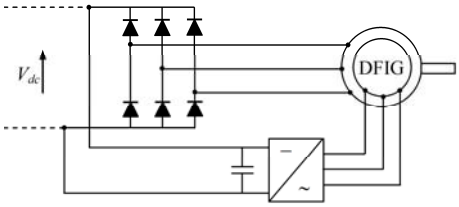

Fig. 1. Conversion topology for a DFIG connected to a DC grid.

The DFIG in Fig. 1 should be designed in order to have a rotor rated magnetomotive force (MMF) higher than the stator MMF, because the magnetization current is supplied only by the rotor. If a DFIG with a inadequate rated rotor MMF is used, the connections can be reversed, namely: the rectifier and the inverter can be connected to the rotor and stator, respectively. It should also be noticed that the choice of the side (stator or rotor) which supplies the magnetizing current does not significantly affect the total size of the DFIG [32].

Even if the study of the low-voltage ride-through is outside the scope of the paper, it is interesting to notice that, differently from a DFIG connected to an ac grid [11]-[12], a dip in the dc grid voltage does not produce over-voltages at the rotor terminals. In fact, the free-wheeling diodes inside the PWM converter immediately clamp the rotor voltage to the low value of the DC voltage. Of course, during a dip in the dc voltage, the PWM converter should be carefully protected from over-currents.

III. DFIG Model

By considering a generic frame *dq*, the sign of the currents in Fig. 2 together with a positive torque in the operation as generator, as well as the peak values of the stator rated voltage and current as fundamental base quantities, the DFIG equations in per-unit (p.u.) are:

$$\bar{v}_s = -R_s \bar{i}_s + \frac{1}{\omega_b}\frac{d\bar{\psi}_s}{dt} + j\frac{1}{\omega_b}\frac{d\theta_s}{dt}\bar{\psi}_s \qquad (1)$$

$$\bar{v}_r = R_r \bar{i}_r + \frac{1}{\omega_b}\frac{d\bar{\psi}_r}{dt} + j\frac{1}{\omega_b}\frac{d\theta_r}{dt}\bar{\psi}_r \qquad (2)$$

$$\bar{\psi}_s = M\bar{i}_r - L_s\bar{i}_s \;\;,\;\; \bar{\psi}_r = L_r\bar{i}_r - M\bar{i}_s \;\;,\;\; t_e = \mathrm{Im}(\bar{i}_s \underline{\psi}_s)\,. \qquad (3)$$

By introducing an arbitrary factor *a*, equations (1)-(3) can be formally rewritten by using transformed rotor quantities [33]

$$\bar{v}_r' = a\,\bar{v}_r \;\;,\;\; \bar{\psi}_r' = a\,\bar{\psi}_r \;\;,\;\; \bar{i}_r' = \bar{i}_r/a\,, \qquad (4)$$

$$R_r' = a^2 R_r \;\;,\;\; L_{as} = L_s - aM \;\;. \qquad (5)$$

Equations (1)-(5) lead to the most general equivalent circuit shown in Fig. 2 by considering the stator frame. The electromotive force $\bar{e}_x'$ is due to the flux $\bar{\psi}_x'$, which corresponds to a fraction of the transformed rotor flux linkage $\bar{\psi}_r'$. The value of $\bar{\psi}_x'$ is given by

$$\bar{\psi}_x' = \bar{\psi}_s + L_{as}\bar{i}_s \;\;. \qquad (6)$$

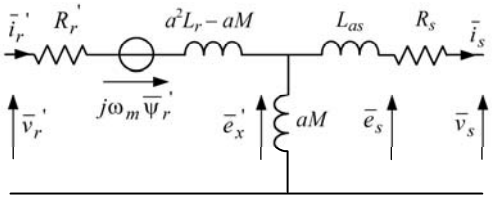

Fig. 2. General equivalent circuit of the DFIG depending on the factor *a* and by considering the stator frame.

IV. Regulation of the DC power

A. Basic background

Generally, in grid connected wind generators, a Maximum Power Point Tracking (MPPT) algorithm provides the reference speed or the reference torque to be realized by the DFIG control. Such an approach can be used also when a rectifier is connected to the stator of the DFIG, if the dc voltage is regulated by other apparatus which share the same dc-bus. Thus, the main aim is to control the power delivered to the dc bus and the frequency of the DFIG, which should be kept near the rated value, in order to meet both the flux and the apparent power capabilities.

A simple control technique for the system in Fig. 1 consists in forcing along a circular trajectory at constant speed the flux $\bar{\psi}_x'$, which corresponds only to a fraction of the flux linked to the rotor windings, according to the choice of *a* in (4)-(6). Using $\bar{\psi}_x'$ instead of $\bar{\psi}_s$ introduces the leakage inductance L_{as} as additional decoupling element between the diode bridge and an equivalent three-phase sinusoidal EMF system. The steady state equivalent circuit of the stator is represented in Fig. 3, which is immediately deduced from the equivalent circuit in Fig. 2.

The behavior of a diode rectifier connected to a dc constant voltage source in Fig. 3 has been thoroughly analyzed in [34]-[35].

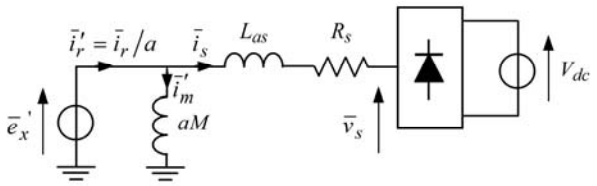

Fig. 3. Steady-state equivalent circuit for the DFIG stator connected to the rectifier.

It has been shown that the system exhibits several operation modes: their occurrence depends on the ratio *m* between the dc voltage and the amplitude of the ac phase voltage. By considering the amplitude-invariant Park transformation and the p.u. values, the ratio *m* can be expressed in terms of the p.u. dc voltage V_{dc} and of the p.u. amplitude of the ac voltage $\bar{e}_x'$ or of the p.u. flux space vector $\bar{\psi}_x'$ in the following form:

$$m = V_{dc}\big/\left|\bar{e}_x'\right| = V_{dc}\big/\left(\omega_s\psi_x'\right) \;\;. \qquad (7)$$

The waveforms of the stator current and of the ac EMF in the stator phase "a" for the main meaningful operation modes are shown in Fig. 4 (the mode 2/3/2/0 is neglected [34]). Mode 3/3 is also called continuous conduction mode (CCM).

If $a < L_S/M$ there is some (positive) leakage inductance between the rectifier and the internal sinusoidal EMF obtained by forcing the flux ψ'_x along a circular trajectory. It will be proven that the most advantageous choice of a makes the resulting p.u. leakage inductance L_{as} significantly higher than the p.u. stator resistance, hence R_s is neglected in this analysis.

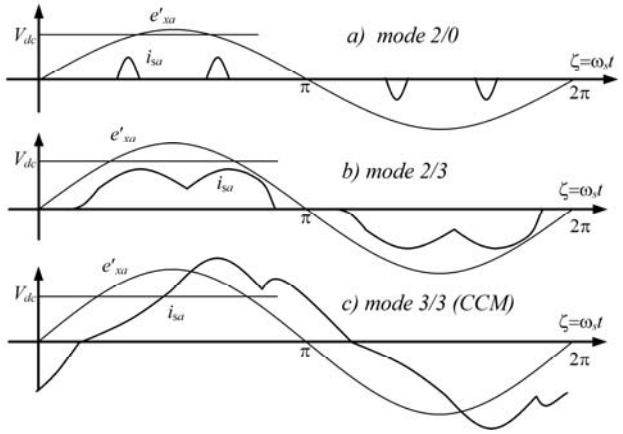

Fig. 4. Steady state waveforms for the system in Fig. 3. (a) mode 2/0 (discontinuous), (b) mode 2/3 (with overlapping conductions), (c) mode 3/3 (continuous conduction mode, (CCM)).

In such a condition, according to [34], the p.u. power P_{dc} delivered to the dc-bus and the p.u. rms stator current $I_{s\,rms}$ can be expressed as

$$P_s = \frac{\psi'^2_x}{L_{as}}\omega_s g_P(m) \quad , \quad I_{s\,rms} = \frac{\psi'_x}{L_{as}} g_I(m) \ . \qquad (8)$$

In (8), L_{as} is the p.u. transformed stator leakage inductance (5b), ω_s is the p.u. stator frequency, whereas $g_I(m)$ and $g_P(m)$ are suitable functions. Their trends versus m are shown in Fig. 5 together with the boundary values of m which delimit the various operation regions.

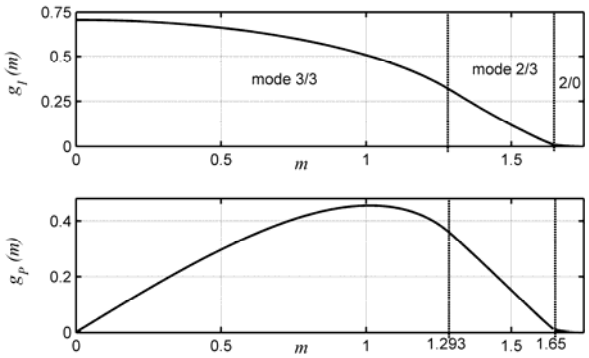

Fig. 5. Trend of $g_I(m)$ and $g_P(m)$ in (8) for the whole range of m $[0,\sqrt{3}]$.

As shown in [34], the exact definitions of $g_I(m)$ and $g_P(m)$ are available only in implicit form and depend on the mode of operation of the rectifier. For control purposes, as it will be shown, only the mode 2/3 is interesting. It occurs when $9/(9+4\pi^2)^{1/2} < m < 1.654$ where $g_I(m)$ and $g_P(m)$ are well approximated by:

$$g_I(m) = 0.46816\,m^3 - 1.59643\,m^2 + 0.79014\,m + 0.94575 \ , \qquad (9)$$

$$g_P(m) = 0.95379\,m^3 - 4.20566\,m^2 + 5.1764\,m - 1.36976 \ . \qquad (10)$$

Equation (8a) states that the stator power and then also the average electromagnetic torque can be regulated by varying the amplitude of the flux linkage ψ_x' .

The performances which can be achieved by using different values of a should be compared by considering the operation within the capability limits of the DFIG.

The first constraint to be considered concerns the limit of the saturation level. In a simplified analysis, the peak value $\psi_{s\,pk}$ of the (distorted) stator flux linkage can be assumed as representative of the degree of saturation in the DFIG. The value of $\psi_{s\,pk}$ should not exceed the rated value 1.0 p.u., which would correspond to the sinusoidal operation of the DFIG at rated stator voltage. Since $R_S \approx 0$, the stator voltage is roughly the derivative of the stator flux linkage, so that the peak value $\psi_{s\,pk}$ can be evaluated by halving the integral of the stator voltage between two of its consecutive zero points. In a large range of operation in mode 2/3 and in mode 2/0 (i.e. for $9/(9+4\pi^2)^{1/2} < m < \sqrt{3}$ [34]), the stator current is clamped to zero in a relatively large neighborhood of $\zeta=0$ (see Fig. 4b). Thus, the integral can be performed in $(0,\pi)$ producing the trivial result

$$\psi_{s\,pk} = \frac{1}{2}\int_0^{\pi}\left(\omega_s\psi'_x \sin\zeta - \omega_s L_{as}\frac{di}{d\zeta}\right)d\zeta = \omega_s\psi'_x \ . \qquad (11)$$

When m is close to the CCM boundary ($m = 9/(9+4\pi^2)^{1/2} \approx 1.293$ [34]-[35]), (11) does not hold, because the stator current is no longer clamped to zero in a neighborhood of $\zeta=0$. It can be proven that (11) is exact for $m \geq 1.527$, and gives an error less than 3.5% for $1.4 \leq m \leq 1.527$.

The second constraint regards the current limits: since here the magnetization current is entirely supplied from the rotor, the most restrictive constraint concerns the rotor current. Considering the equivalent circuit in Fig. 2 and Fig. 4c as well as the operation at the rated frequency (ω_s=1 p.u.) , the p.u. rms value $I_{r\,rms}$ of the rotor current is

$$I_{r\,rms} = a\sqrt{I^2_{s\,rms} + \frac{1}{2}\left(\frac{\psi'_x}{aM}\right)^2 + 2\frac{\psi'_x/\sqrt{2}}{aM} I_{s1\,rms}\sin\varphi_1} \ . \qquad (12)$$

The last term in the radicand involves the rms value $I_{s1\,rms}$ of the first harmonic stator current component and its phase displacement φ_1. Considering the p.u. stator power P_s, it can be deduced

$$I_{s1rms}\cos\varphi_1 = \frac{P_s}{\sqrt{2}\psi'_x} = \sqrt{I_{s1rms}^2 - \left(I_{s1rms}\sin\varphi_1\right)^2} \quad . \quad (13)$$

By using the approximation $I_{s1rms}^2 \approx I_{srms}^2$, (13) can be solved with respect to $I_{s1\,rms}\sin\varphi_1$. Replacing this in (12) and using (8) yields

$$I_{r\,rms} \cong a\left(\left(\frac{\psi'_x}{L_{as}}g_I(m)\right)^2 + \frac{1}{2}\left(\frac{\psi'_x}{aM}\right)^2 + \frac{\psi'^{\,2}_x}{aML_{as}}\sqrt{2g_I^2(m) - g_P^2(m)}\right)^{1/2} \quad . \quad (14)$$

By considering (8) as well as the constraints ψ_x'= 1 p.u. (due to (11)) and (15) with $I_{r\,rms} = ((I_{rn}/n_{12})/I_{sn})/\sqrt{2}$ p.u. (I_{rn}/n_{12} is the rated rotor current referred to the stator), we can compare the effect of the choice of a on the performances of the system in Fig. 3 when the DFIG is operating at its capability limits.

B. Choice of the optimal value of the factor a

The value of a (or L_{as}) is a degree-of-freedom which can be exploited to minimize the derating of the DFIG, i.e. to minimize the reduction of the exploitable power with respect to the sinusoidal operation, as a consequence of the harmonics as well as of the phase shift of the stator current. It turns out to be more advantageous to express both a and L_{as} as a function of m and use this as independent variable. To this purpose, (5b) and (14) equated to $k/\sqrt{2}$ p.u. (rotor current constraint, k= $(I_{rn}/n_{12})/I_{sn}$) and with ψ_x'=1 p.u., allow to find L_{as} and a as a function of m:

$$L_{as} = \frac{L_s}{1+g_L(m,M)} \quad , \quad a = \frac{L_s}{M}\frac{g_L(m,M)}{1+g_L(m,M)} \quad , \quad (15)$$

where

$$g_L(m,M) = \frac{\sqrt{2g_I^2(m) - g_P^2(m)}}{2g_I^2(m)}\left(-1+\sqrt{1+\frac{2\left((kM)^2 - \psi'^{\,2}_x\right)\,g_I^2(m)}{\left(2g_I^2(m) - g_P^2(m)\right)\psi'^{\,2}_x}}\right). \quad (16)$$

By using (15a), the p.u. power (8a) delivered to the dc-bus at the rated frequency and flux becomes

$$P_s = \frac{1}{L_s}(1+g_L(m,M))\,g_P(m). \quad (17)$$

The value of m which maximizes (17) represents the operation point with maximum power-per-ampere (rotor). As an example, Fig. 6 reports the trends of P_s (17) and L_{as} (15a) versus m in the range of the operation mode 2/3 by supposing k=1 (i.e. equal rated stator and rotor MMF): various values of M are considered and a constant stator leakage $L_s - M$ = 0.08 p.u. is assumed.

The curves of P_s exhibit a quite flat maximum: for ordinary values of M, the optimal value m_{opt} belongs to the range 1.45 < m_{opt} <1.56. Hence, it can be advantageous to operate with m slightly lower than the optimal value, in order to increase the commutation inductance. The magnetization inductance M has a strong effect on the performances: In small DFIGs, which have typically $M \le 2$ p.u., the derating is significant. Case $M = \infty$ has only a theoretical interest: the related maximum power equals 0.92 p.u.. The optimal value of L_{as} belongs to the range 0.1 p.u. ≤ L_{as} ≤ 0.25 p.u. from large to small DFIG: these values justify the assumption $R_s \approx 0$ invoked in the analysis. In the aforementioned example, the following optimal values arise (see Fig. 6): m_{opt} =1.557 and L_{as} =0.126 p.u.. Moreover, as shown in Fig. 6(a), the maximum stator power compatible with the DFIG capability limits is P_S = 0.766 p.u.. In order to evaluate the actual derating due to the rectifier, it should be noticed that in the sinusoidal operation at rated voltage and with the stator current in phase with the stator voltage, it would be $P_S \approx \sqrt{(1-1/M^2)} = 0.94$ p.u..

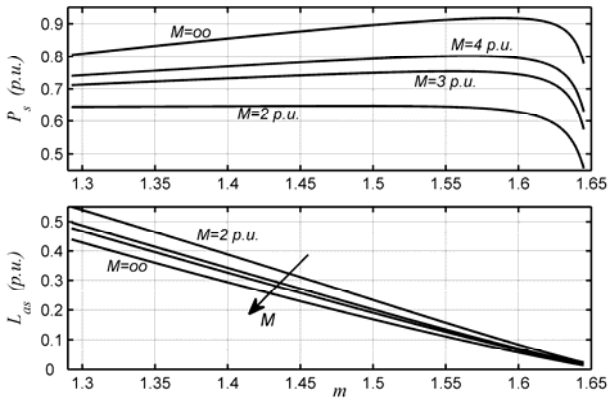

Fig. 6. Trend of P_s (17) and L_{as} (15a) in the operation mode 2/3 (ψ'_x=1 p.u.).

C. Choice of the DFIG rated voltage and turn-ratio

If the system in Fig. 1 is to be connected to an existing dc-grid with a given voltage $V_{dc}^{(Volt)}$ (in Volt), the most appropriate rated stator voltage V_{sn} (line-to-line, rms) as well as the stator/rotor turn ratio n_{12} of the DFIG have to be chosen. After setting m to the optimal value in the rated conditions, the p.u. dc voltage V_{dc} is determined by (7) with ψ'_x =1 p.u. and ω_s =1 p.u.. Since the base voltage is $\sqrt{(2/3)}V_{sn}$, it results:

$$V_{dc} = m \quad \Rightarrow \quad V_{sn} = \sqrt{3/2}\;V_{dc}^{(Volt)}\big/m \quad . \quad (18)$$

Due to (18), the rated rotor voltage V_{rn} should be

$$V_{rn} = \frac{|s|_{\max}}{n_{12}}V_{sn} = \frac{|s|_{\max}}{n_{12}}\sqrt{\frac{3}{2}}\frac{V_{dc}^{(Volt)}}{m} \quad , \quad (19)$$

where $|s|_{max}$ is the maximum slip and n_{12} is the stator/rotor turn ratio. The rated rotor voltage must be lower than the maximum ideal rms line-to-line ac voltage which can be obtained at the rotor side by the space vector modulation using the dc voltage $V_{dc}^{(Volt)}$; thus: $V_{rn} < V_{dc}^{(Volt)}/\sqrt{2}$. Introducing this value in (19) provides the inferior limit for the turn ratio n_{12} when the stator diode rectifier and the rotor inverter have to be connected to the same dc-bus

$$n_{12} > \sqrt{3}|s|_{\max} / m \cong 0.37 \ . \tag{20}$$

In (20) the values m = 1.54 and $|s|_{max}$ = 0.33 have been assumed. In order to provide a margin for the voltage drops across the rectifier and the inverter as well as for the dynamic regulation, a turn ratio n_{12} slightly higher than the limit (20) should be required.

V. Implementation of the Control

The control scheme is shown in Fig. 7. The reference angle θ_s^* of the control reference frame is generated by integrating a constant angular frequency ω_s^* equal to the rated frequency of the DFIG [36]. Such an angle is used together with the mechanical position θ_m to find the slip angle which must be used in the frame transformations of the rotor currents and voltages. The field orientation along $\overline{\psi}_x$ is achieved by forcing $\psi_{xq}^* = 0$. Here θ_m is measured by an encoder, however it could also be estimated by an observer [4]-[10]. Since the system in Fig. 1 does not supply other ac loads, an accurate dynamic regulation of the frequency during the fluctuation of the prime mover torque is not needed.

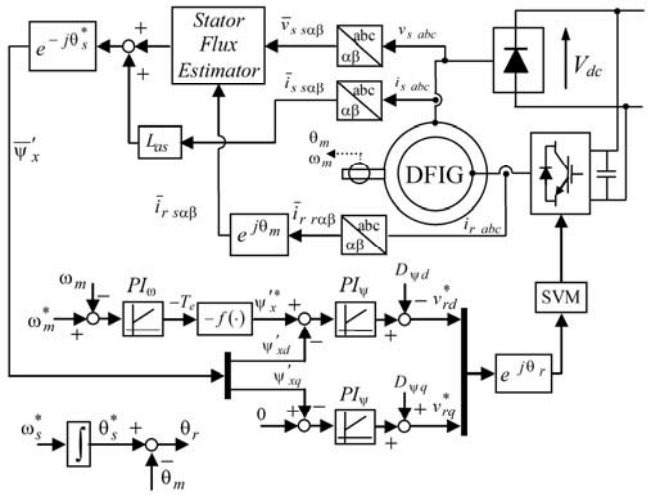

Fig. 7. Proposed control scheme. The negative sign in the block $f(\cdot)$ is due to the fact that the PI_ω provides the reference moving torque demand, i.e. $-T_e$.

The reference fluxes $\psi_{xd}^* = \psi_x^*$ and $\psi_{xq}^* = 0$ are tracked by PI controllers acting on the rotor voltages. From (3)-(6), the following relation between $\overline{\psi}_r$ and $\overline{\psi}'_x$ can be deduced:

$$\overline{\psi}_r = \overline{\psi}'_x / a + (L_r - M/a)\,\bar{i}_r \ . \tag{21}$$

By using (21), the rotor equation (2) becomes

$$\bar{v}_r = \frac{1}{a}\frac{1}{\omega_b}\frac{d\overline{\psi}'_x}{dt} + \overline{D}_\psi \ , \tag{22}$$

where

$$\overline{D}_\psi = R_r \bar{i}_r + j\omega_r \overline{\psi}'_x / a + \\ + j\omega_r (L_r - M/a)\bar{i}_r + (L_r - M/a)\frac{1}{\omega_b}\frac{d\bar{i}_r}{dt} \ . \tag{23}$$

The quantity $\overline{D}_\psi$ collects the decoupling terms for the flux control loops: In the implementation, the time derivative of $\bar{i}_r$ in (23) must be approximated by a high-pass filter.

The flux linkage $\overline{\psi}'_x$ used as feedback is deduced by (6), which must be transformed on the control frame by the angle θ_s^*. The stator flux linkage in (6) is computed by the integral of the stator EMF: to avoid the drift, an approximate integrator [5] or a formulation involving a decay term [36] can be used.

The value of ψ'^*_x is deduced from the torque demand. For control purposes, the trend of g_P (m) in Fig. 5 can be effectively approximated by a straight-line whose equation is

$$g_P(m) \cong c_1 - c_2 m \quad , \quad c_1 = 1.613 \ , \quad c_2 = 0.974 \ . \tag{24}$$

According to (7)-(8) and (24), the stator power can be expressed as a function of the flux amplitude ψ_x' by:

$$P_s \cong \frac{\omega_s \psi_x'}{L_{as}}(c_1 \psi_x' - c_2 \frac{V_{dc}}{\omega_s}) \ . \tag{25}$$

The value of the set-point flux $\psi_x'^*$ which corresponds to the desired average torque T_e is obtained by replacing the steady state relation $P_s = \omega_s T_e$ in (25) and by solving the final expression with respect to $\psi_x' = \psi_x'^*$:

$$\psi'^*_x = f(T_e) \equiv \frac{c_2}{c_1}\frac{V_{dc}}{2\omega_s}\left(1 + \sqrt{1 + \frac{4\,c_1\,L_{as}}{(c_2 V_{dc}/\omega_s)^2} T_e}\right) \ . \tag{26}$$

The function $f(\cdot)$ (with ω_s =1 p.u.) is useful to implement a speed loop control, where the reference torque is the output of a PI speed controller (PI_ω in Fig. 7). Using $f(\cdot)$, the design of the PI_ω becomes independent of the operation point. For ordinary values of the quantities in (26), the square root can be linearized.

VI. Simulation Results

In order to validate the theory, a Simulink model has been used to perform some simulations on the system in Fig. 7. A medium-size DFIG has been considered: the parameters are reported in the Appendix. By using the results in Section IV-B

(see Fig. 6, with M=3 p.u.), the optimal values m = 1.556, a = 0.985, and L_{as} = 0.126 (p.u.) have been implemented. Consequently, the dc voltage has been set at 483 V as deduced by (17) with V_{sn} = 380 (V). The previous analysis provides the limit average electromagnetic torque magnitude equal to 0.76 p.u. when the DFIG reaches the rotor current limit. The PI flux and speed regulators have been designed with a bandwidth of 200 Hz and 3 Hz respectively. An ideal inverter controlled by a space vector modulation technique has been used.

Fig. 8 shows the response of the system during some steps in the torque of the prime mover. Initially, the DFIG is driven at synchronism by the dc motor; at t = 0 (s) the control is enabled and the flux quickly reaches a value slightly lower than 1.0 p.u., at t =0.1 (s) a step equal to 0.2 p.u. in the moving torque is applied. A further step is applied at t =2.5 (s) bringing the moving torque to 0.76 (p.u.), which should correspond to the rotor current capability. A final step is delivered at t = 5 (s), by setting the torque at 0.1 (p.u.). After a transient in the speed, according to the bandwidth of the speed loop, the system is able to recover to the set-point speed (1.0 p.u.). It should be noticed that the presence of the diode rectifier does not allow a negative (motoring) torque, thus the deceleration transient can be slower as it happens in the interval 5.3 (s) < t < 6 (s), where the torque demand saturates to zero. By comparing the frequency of the rotor currents and the mechanical speed, it can be concluded that the steady state stator frequency equals the set-point value (50 Hz). The flux components exhibit some ripple due to the low capability of the flux controllers in tracking the harmonic components at 300 Hz and higher. The detail of the stator currents and voltages at steady state just before t =5 (s) is shown in Fig. 9: the rectifier operates in mode 2/3, and, as required, the frequency is 50 Hz. The space vectors related to the 5th harmonic (negative sequence) and the 7th harmonic (positive sequence) of the stator current rotate at $6\omega_b$ with respect to the oriented dq frame and originate the main component (300 Hz) of the torque ripple [18]. The peak-to-peak torque ripple in the electromagnetic torque is about 0.18 p.u. and it is due to the distorted stator currents. By analyzing the stator and rotor current, the global rms values are $I_{s\ rms}$ = 0.58 p.u. and $I_{r\ rms}$ = 0.695 p.u.: as expected, $I_{r\ rms}$ is very close to $1/\sqrt{2}$ = 0.707, which represents the rotor current limit value. The stator voltage is distorted, but this is not a trouble in the considered application.

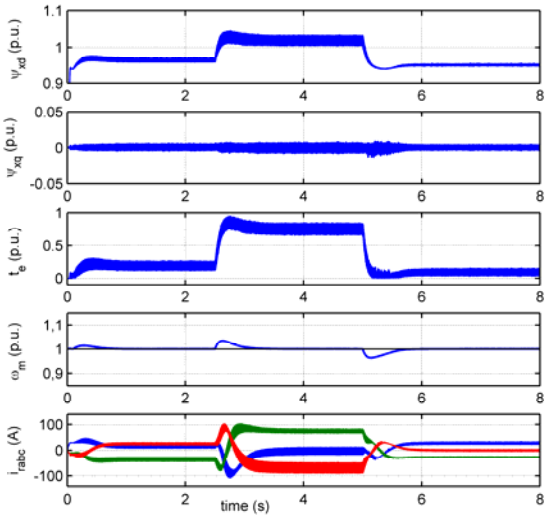

Fig. 8. Behavior at synchronism during some steps in the moving torque.

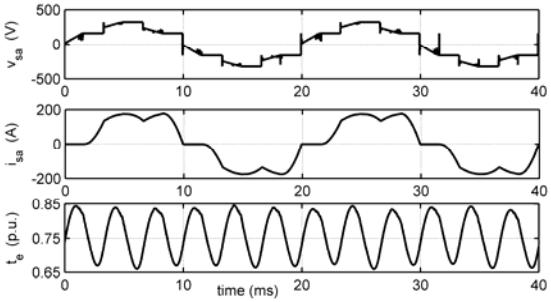

Fig. 9. Detail of the stator currents and voltages and of the electromagnetic torque just before t = 5 (s).

Fig. 10 shows the behavior of the system during some steps in the reference speed and with a constant moving torque equal to 0.5 (p.u.): the reference speed is correctly tracked by the control. The torque demand in the PI_ω is saturated at 1.0 p.u. and this is clearly visible in the second transient.

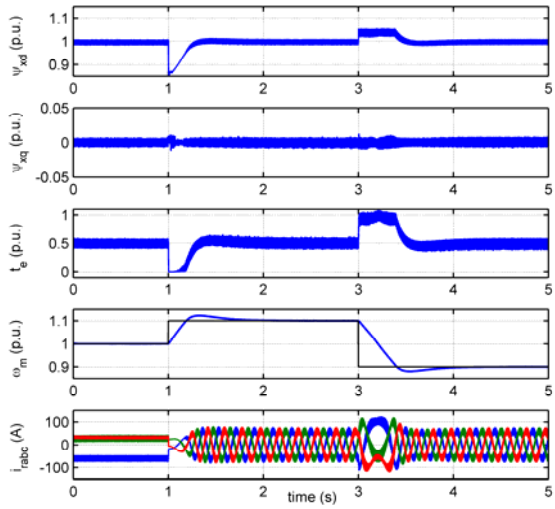

Fig. 10. Response after a variation of the reference speed, with T_L=–0.5 (p.u.).

Finally, Fig. 11 reports the results in the same test conditions of Fig. 8, except for the new values L_{as} = 0.5 (p.u.) and m =

1.293. These values are read in Fig. 6(b) on the curve with M = 3 p.u.: they should bring the diode rectifier in CCM and reduce the torque ripple.

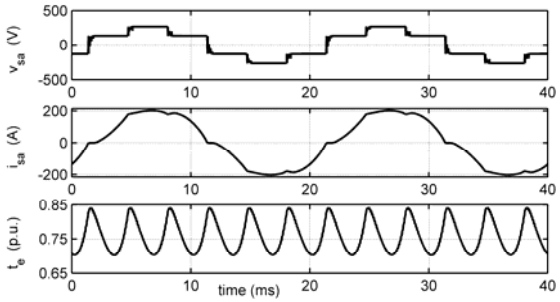

Fig. 11. Results in the same test conditions of Fig. 9 but with L_{as} = 0.5 (p.u.) and m = 1.293.

The operation in quasi-CCM is rather confirmed by Fig. 11, where the torque ripple equals 0.14 p.u.. However, in these conditions, the rotor current capability limit is exceeded: in fact, Fig. 6(a) shows that the maximum tolerable torque with m = 1.293 is 0.71 p.u. instead of 0.766 p.u.. It should be noticed that, in this last test, L_{as} is more than twice $L_{ks} = \sigma L_S$ =0.195 p.u.. Then, the system can operate also with a negative transformed rotor leakage inductance $a^2L_r - aM$.

The comparison between Fig. 11 and Fig. 9 shows that the increase of L_{as} can be exploited in order to reduce the torque ripple: L_{as} can be increased via software, without using an external physical inductor. However as shown in Fig. 6, a higher L_{as} increases the derating of the DFIG.

Some alternative control schemes for DIFGs connected to a distorted ac grid or feeding non-linear loads work in the stator flux frame and use resonant controllers to track the harmonic at 300 Hz in the q-axis reference rotor current required to compensate for the torque ripple [19]-[21]. However, such a method can even increase the distortion in the stator current and the ripple in the stator power, which is the main part of the power delivered to the dc bus [19]. The compensation of the harmonics can be obtained by restoring the grid-side converter and by using it as an active filter [23],[4],[37]. Such a solution is effective: however, with respect to the layout in Fig. 1, it needs an additional PWM converter and suitable decoupling reactors. A technique to mitigate the torque ripple suitable for the layout in Fig. 1 and for the control method here proposed consists in using a twelve-pulse rectifier instead of a six-pulse one. This requires to split the stator winding into two suitable three-phase windings, which feed two three-phase diode rectifiers in parallel on the same dc-bus. The torque ripple components due to each sub-system are roughly halved and they are in opposition, so that the resulting torque ripple is considerably reduced. Some tests performed in [38] and dealing with a PMSG showed that twelve-pulse rectifier configurations produce a torque ripple which is about a fourth of that one in six pulse systems.

VII. Experimental results

Fig. 12 reports the layout of the experimental setup. The 3.7 kW DFIG whose data are given in the Appendix is coupled to a dc machine which works as prime mover. Since n_{12}=2.05, in order to obtain a turn ratio near the value (20) the roles of the stator and of the rotor have been exchanged between each other, so that the turn-ratio between the rectifier and the inverter sides is 1/2.05=0.49. This way, also the higher rated MMF of the stator can be exploited to supply the magnetization current. Thus, the DFIG rotor is connected through a three-phase uncontrolled bridge to a dc-bus whose voltage is generated by another dc machine (30 kW 250V). Such a dc machine is coupled to a Squirrel Cage Induction Machine (SCIM) which allows the regenerative operation. By using the parameters in the Appendix, the implemented optimal values (20) are: m = 1.52 and L_{as} = 0.19 (p.u.). Hence, using (18), the dc-bus has been regulated at 230 V. The cross-over frequencies of the flux and speed loops have been set at 200 Hz and 3 Hz respectively. The control routine has been implemented on a DSpace board (DS 1103) housed in a host PC using a sampling/switching frequency of 10 kHz.

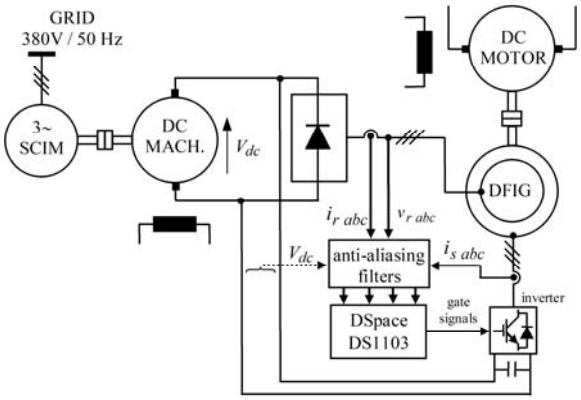

Fig. 12. Layout of the experimental setup. In order to obtain a turn ratio near the value in (20), the diode rectifier has been connected to the rotor.

Fig. 13 shows the response of the system to a step in the reference speed from 1.0 to 0.9 p.u. in such a way to obtain a final moving torque equal to 0.5 p.u., according to the torque curve of the dc motor (whose armature is fed by a diode rectifier and a variac). The steady state speed error is zero and the speed transient matches with the designed bandwidth of the speed loop. Correspondingly, the d-axis reference stator flux changes in order to produce the necessary torque. The q-axis reference flux is maintained at zero and proves that the field orientation is achieved. The frequency of the stator (inverter) currents is coherent with the mechanical speed and with the reference rotor (rectifier side) frequency. Similar results have been obtained for an increasing step in the reference speed.

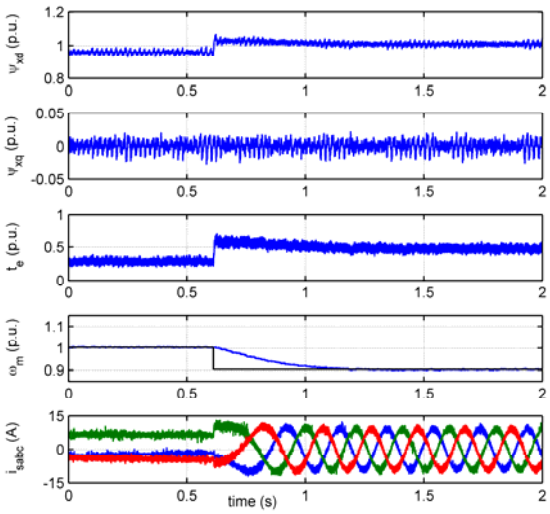

Fig. 13. Response to some steps in the speed reference.

The response to a step in the moving torque from about 0 p.u. to about 0.5 p.u. (near the limit of saturation of the anti-windup speed controller) when ω_m^* =1 p.u. is reported in Fig. 14. Since the system is speed regulated, a perturbation in the torque produces a transient in the speed, whose dynamics is related to the low cross-over frequency of the speed loop. Nevertheless, the system is able to restore the speed and the rotor (rectifier side) frequency at the set-point value. Similar results have been obtained at different reference rotor speeds: namely ω_m^* = 0.9 p.u., and ω_m^* = 1.1 p.u., again by delivering a step in the moving torque from about 0 p.u. to 0.5 p.u.. Results are shown in Figs. 15 and 16, respectively. In all the tests the system tracks the reference speed and frequency.

Fig. 17 reports the response to a step in the moving torque from 0.5 p.u. to zero. This is obtained by reducing the armature voltage of the dc motor coupled to the DFIG. It should be noticed that, as expected, the control cannot maintain the desired speed, because the moving torque is not high enough. Hence the DFIG slows until a new mechanical equilibrium between friction torque and moving torque is reached. However, this test proves that the system works ("sleeps") stably even with zero electromagnetic torque. In this case, the control forces the minimal value of the flux ψ_{xd}' which arises from the saturation set in the anti-windup speed controller, through (26).

The details of the steady-state rotor (rectifier side) phase voltage and current for T_e = 0.5 p.u. and ω_m^* = 1.0 p.u. are reported in Fig. 18. As predicted by the theory, the diode bridge operates in mode 2/3, moreover the desired frequency is obtained (50 Hz). The high frequency peak to peak torque ripple is about 0.18 p.u..

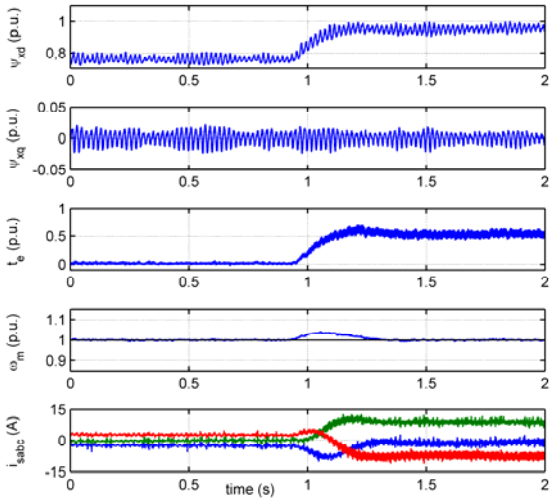

Fig. 14. Response to a step in the moving torque at synchronism.

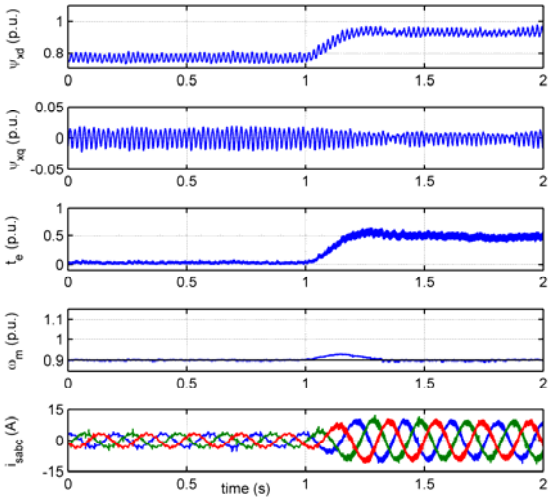

Fig. 15. Response to a step in the moving torque when ω_m^* = 0.9 p.u..

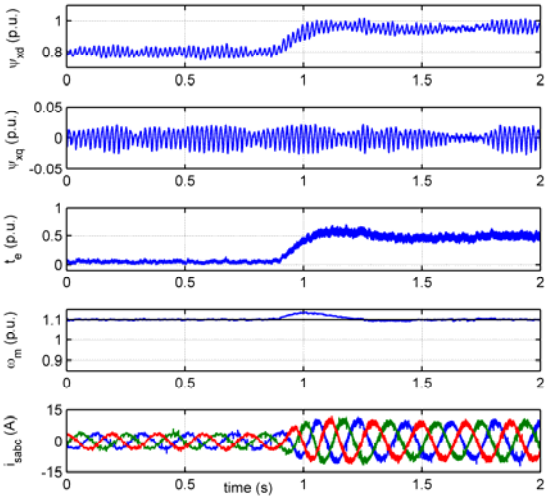

Fig. 16. Response to a step in the moving torque when ω_m^* = 1.1 p.u..

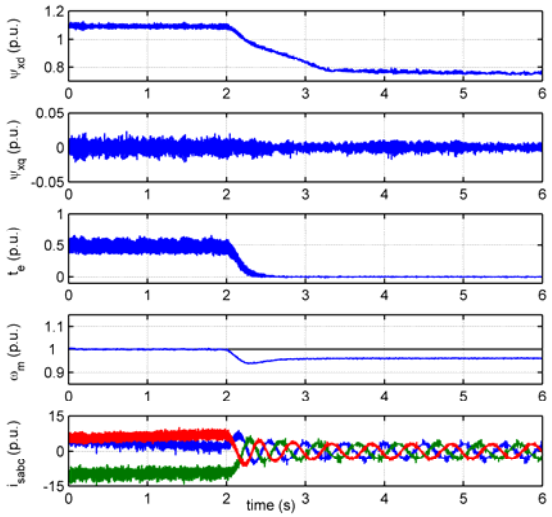

Fig. 17. Behavior with zero electromagnetic torque, when the moving torque is not enough to allow the speed regulation.

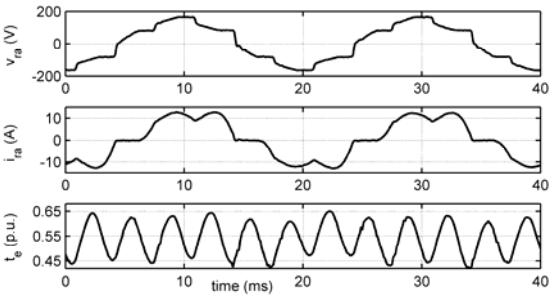

Fig. 18. Details of the rotor phase voltage and current and of the electromagnetic torque at steady state.

In order to experimentally prove the attitude of the system to work even with a negative transformed rotor leakage inductance, Fig. 19 reports the details of the rotor voltage and current and of the electromagnetic torque in the same test conditions of Fig. 13, but with L_{as} = 0.54 (p.u.) and m = 1.293. Theoretically, these values should produce incipient CCM, actually, Fig. 17 shows that the system still operates in mode 2/3. This disagreement can be imputed to the high rotor resistance which drops the boundary value of m [34]. Nevertheless, the benefic effect of a high L_{as} is evident: in fact the torque ripple is drooped to about 0.1 p.u., i.e. it is almost halved with respect to the case with L_{as} = 0.19 p.u. (Fig. 18).

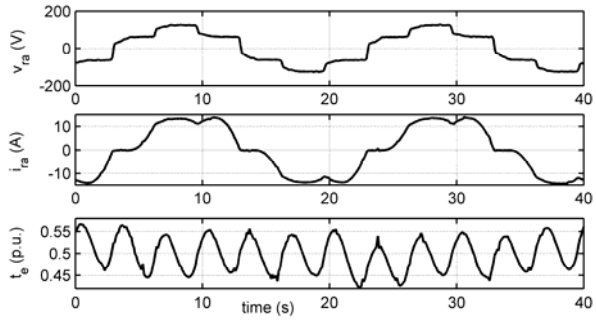

Fig. 19. Results in the same test conditions of Fig. 18 but with L_{as} = 0.54 (p.u.) and m = 1.293. The torque ripple is almost halved.

The harmonic content of the steady-state rotor and stator currents in the tests of Figs. 18 and 19 is reported in Table I.

TABLE I
HARMONIC CONTENT OF THE STATOR AND ROTOR CURRENTS FOR THE TESTS IN FIGS. 18 AND 19.

L_{as} (p.u.)	h	5	7	11	13	17	19	THD
0.19	I_{rh} / I_{r1} (bridge)	0.244	0.072	0.034	0.029	0.012	0.015	0.259
	I_{sh} / I_{s1} (inv. †)	0.129	0.034	0.021	0.015	0.005	0.006	0.137
0.54	I_{rh} / I_{r1} (bridge)	0.168	0.072	0.023	0.016	0.011	0.009	0.186
	I_{sh} / I_{s1} (inv. †)	0.121	0.054	0.018	0.012	0.005	0.005	0.134

† current transformed in the rotor (bridge-side) frame, to have a 50 Hz signal

Since the DFIG is at synchronism, the fundamental component of the stator (inverter) current is in dc. In order to allow an easy comparison between the stator and the rotor harmonics, the stator (inverter) current has been transformed on the rotor frame, before performing the analysis. Table I confirms the lower distortion of the currents when the commutation inductance L_{as} is higher. Moreover, the stator (inverter) currents are less distorted than the rotor (diode bridge) ones.

VIII. CONCLUSION

A new conversion topology for DFIGs connected to a dc-bus has been considered in this paper. In this system an uncontrolled diode rectifier is connected to the stator of the DFIG and shares the same dc-bus of the rotor side inverter. No other converters are required and this feature yields considerable savings in costs and volume. The system is suitable for dc micro-grids where several sources and storages are connected in parallel to the same dc-bus. A scheme for the control of the power delivered to the dc-bus acting on the amplitude of a suitable flux space vector has been proposed: such a flux is a fraction of the rotor flux linkage. Its optimal definition as well as the optimal value of the fraction of the leakage inductance to be exploited as commutation inductance have been deduced in order to minimize the DFIG derating due to the stator current distortion and phase shift. The effectiveness of the control has been proven by simulations and by some experimental tests.

APPENDIX

Parameters of the DFIG used in the simulations: 100 (kW), 380 (V), 158 (A), 50 (Hz), 4 poles, turns ratio n_{12} = 0.4, M = 3.00 (p.u.), L_r = 3.12 (p.u.), L_S = 3.08 (p.u.), R_r = 0.01 (p.u.), R_S = 0.01 (p.u.), inertia constant H = 0.45 (s).

Parameters of the DFIG used in the experimental tests: (stator Y /rotor Y) 380/185 (V), 8/12.5 (A), 3.75 (kW), 50 (Hz), 4 poles, turns ratio n_{12} = 2.05, M = 2.13 (p.u.), L_r = 2.25 (p.u.), L_S = 2.27 (p.u.), R_r = 0.071 (p.u.), R_S = 0.057 (p.u.), inertia constant (including the DC motor) H = 0.28 (s).

REFERENCES

[1] R. Cárdenas, R. Peña, S. Alepuz, G. Asher, "Overview of control systems for the operation of DFIGs in wind energy applications," IEEE Trans. Ind. Electron., vol. 60, n° 7, pp. 2776-2798, July 2013.

[2] R. Pena, J. C. Clare, and G. M. Asher, "Doubly fed induction generator using back-to-back PWM converters and its application to variable-speed wind-energy generation", Proc. Inst. Elect. Eng. –Elect. Power Appl., vol. 143, pp. 231-241, May 1996.

[3] H. Nian, Y. Song, "Direct power control of doubly fed induction generator under distorted grid voltage," *IEEE Trans. Power Electron.*, vol. 29, no. 2, pp. 894–905, Feb. 2014.

[4] A. Kumar Jain, V.T. Ranganathan, "Wound Rotor Induction Generator with Sensorless Control and Integrate Active Filter for Feeding Nonlinear Loads in a Stand-Alone Grid," *IEEE Trans. on Ind. Electron.*, vol. 55, No.1pp. 218 – 228, Jan. 2008.

[5] R. Cárdenas, R. Pena, J. Clare, G. Asher, J. Proboste "MRAS Observers for sensorless control of Doubly-Fed Induction Generators," *IEEE Trans. Power Electron.*, vol. 23, No.3, pp. 1075 – 1084, May 2008.

[6] S. Shen, B. Mwinyiwiwa, Y. Zhang, B.T. Ooi, "Sensorless Maximum Power Point Tracking of Wind by DFIG Using Rotor Position Phase Lock Loop (PLL)," *IEEE Trans. Power Electron.*, vol. 24, No.4, pp. 942–951, Apr. 2009.

[7] G. D. Marques, D. M. Sousa, "Air-gap power vector based sensorless method for DFIG control without flux estimator", *IEEE Trans. Ind. Electron.*, vol. 58, no. 10, pp. 4717-4726, Oct. 2011.

[8] G. D. Marques, D. M. Sousa, M. F. Iacchetti, "Open Loop Sensorless Slip Position Estimator of a DFIM Based on Air-gap Active Power Calculations – Sensitivity Study" *IEEE Transactions on Energy Conversion*, vol. 28, no 4, pp. 959-968, Dec. 2013.

[9] M. F. Iacchetti, G. D. Marques, R. Perini, D. M. Sousa, "Stator Inductance Self-Tuning in an Air-gap Power Vector Based Observer for the Sensorless Control of Doubly Fed Induction Machines," *IEEE Transactions on Industrial Electronics*, vol. 61, no 1, pp. 139-148, Jan. 2014.

[10] F. Castelli-Dezza, G. Foglia, M. F. Iacchetti, and R. Perini, "An MRAS observer for sensorless DFIM drives with direct estimation of the torque and flux rotor current components," *IEEE Trans. Power Electron.*,vol. 27, no. 5, pp. 2576–2584, May 2012.

[11] F. K. A. Lima, A. Luna, P. Rodriguez, E. H. Watanabe, F. Blaabjerg, "Rotor voltage dynamics in the doubly fed induction generator during grid faults," *IEEE Trans. Power Electron.* , vol. 25, No.1, Jan. 2010 pp. 118–130.

[12] G. D. Marques, D. M. Sousa, "Understanding the DFIG during Voltage Dips", *IEEE Trans. En. Conv.*, vol. 27, no. 2, pp. 421-431, June 2012.

[13] P.S. Flannery, G. Venkataramanan, "A fault tolerant doubly fed induction generator wind turbine using a parallel grid side rectifier and a series grid side converter," *IEEE Trans. Power Electron.* , vol. 23, No.3, May. 2008 pp. 1126–1135.

[14] D. Santos-Martin, J.L. Rodriguez,-Amenedo, S. Arnalte, "Providing ride-through capability to a doubly fed induction generator under unbalanced voltage dips," *IEEE Trans. Power Electron.* , vol. 24, No.7, pp. 1747–1757, July 2009.

[15] S. Hu, X. Lin, Y. Kang, and X. Zou, "An improved low-voltage ride through control strategy of doubly fed induction generator during grid faults," *IEEE Trans. Power Electron.*, vol. 26, no. 12, pp. 3653–3665, Dec. 2011.

[16] C. Liu, D. Xu, N. Zhu, F. Blaabjerg, M. Chen, "DC-voltage fluctuation elimination through a DC-capacitor current control for DFIG converters under unbalanced grid voltage conditions," *IEEE Trans. Power Electron.*, vol. 28, no. 7, pp. 3206–3218, Jul. 2013.

[17] J. Yao, H. Li, Z. Chen, X. Xia, X. Chen, Q. Li, Y. Liao, "Enhanched control of a DFIG-based wind power generation system with series grid-side converter under unbalanced grid voltage conditions," *IEEE Trans. Power Electron.*, vol. 28, no. 7, pp. 3167–3181, Jul. 2013.

[18] L. Fan, S. Yuvarajan, and R. Kavasseri, "Harmonics analysis of a DFIG for a wind energy conversion system," *IEEE Trans. Energy Convers.*, vol. 25, no. 1, pp. 181–190, Mar. 2010.

[19] J. Hu, H. Nian, H. Xu, and Y. He, "Dynamic modeling and improved control of DFIG under distorted grid voltage conditions," *IEEE Trans. Energy Convers.*, vol. 26, no. 1, pp. 163–175, Mar. 2011.

[20] H. Xu, J. Hu, and Y. He, "Operation of wind-turbine-driven DFIG systems under distorted grid voltage conditions: Analysis and experimental validations," *IEEE Trans. Power Electron.*, vol. 27, no. 5, pp. 2354–2366, May 2012.

[21] Changjin Liu, F. Blaabjerg, Wenjie Chen, Dehong Xu, "Stator current harmonic control with resonant controller for doubly fed induction generator," *IEEE Trans. Power Electron*, vol. 27, no. 7, pp. 3207-3220, July 2012.

[22] Van-Tung Phan, Hong-Hee Lee, "Control strategy for harmonic elimination in stand-alone DFIG applications with nonlinear loads," *IEEE Trans. Pow. Electron*, vol. 26, no. 9, Sept. 2011, pp. 2662-2675.

[23] N. Yu, H. Nian, Y. Quan, "Novel DC grid connected DFIG system with active power filter based on predictive current control," *Electrical Machines and Systems Int. Conf. ICEMS 2011,* 22-23 Aug 2011.

[24] G. D. Marques, M. F. Iacchetti, "Stator Frequency Regulation in a Field Oriented Controlled DFIG Connected to a DC Link," accepted for publication on *IEEE Transactions on Industrial Electronics*, February 2014, DOI: 10.1109/TIE.2014.2311403.

[25] F. Blaabjerg, Z. Chen and S. B. Kjaer, "Power electronics as efficient interface in dispersed power generation system", *IEEE Trans. Power Electron.*, vol. 19, no. 5, pp.1184 -1194, 2004.

[26] P. Karlsson and J. Svensson, "DC bus voltage control for a distributed power system", *IEEE Trans. Power Electron.*, vol. 18, no. 6, pp.1405 - 1412, 2003.

[27] Lie Xu, Dong Chen, "Control and operation of a DC microgrid with variable generation and energy storage, " *IEEE Trans. Power. Del.*, vol. 26, no. 4, pp. 2513-2522, Oct. 2011.

[28] H. Kakigano, Y. Miura, T. Ise ,"Low-voltage bipolar-type DC microgrid for super high quality distribution," *IEEE Trans. Pow. Electron.*, vol. 25, no. 12, pp. 3066-3075, Dec. 2010.

[29] N. Holtsmark, H. J. Bahirat, M. Molinas, B. A. Mork, H. K. Hoidalen, "An All-DC Offshore Wind Farm With Series-Connected Turbines: An Alternative to the Classical Parallel AC Model?" *IEEE Trans. Ind. Electron.*, vol. 60, no. 6, pp. 2420-2428, June 2013.

[30] F. Deng, Z. Chen, "Control of improved full-bridge three-level DC/DC converter for wind turbines in a DC grid," *IEEE Trans. Power Electron.*, vol. 28, no. 1, pp. 314–324, Jan. 2013.

[31] I. Jadric, D. Borojevic, M. Jadric, "Modeling and control of a synchronous generator with an active DC load, " *IEEE Trans. Power Electron.*, vol. 15, no. 2, pp. 303–311, Mar. 2000.

[32] I. Boldea, S. A. Nasar, The induction machine handbook. CRC Press, 2002, chapter 16.

[33] P. Vas, "Vector control of AC machines," Clarendon Press, Oxford, 1990, pp 146-147.

[34] A. Di Gerlando, G. M. Foglia, M. F. Iacchetti, R. Perini, "Comprehensive steady-state analytical model of a three-phase diode rectifier connected to a constant DC voltage source," *IET Power Electronics*. Vol. 6, no. 9, pp. 1927-1938, Nov. 2013.

[35] Bleijs, J. A. M.: 'Continuous conduction mode operation of three-phase diode bridge rectifier with constant load voltage', *IEE Proc. Electr. Power Appl.*, vol. 152, no. 2, pp. 359-368, Mar. 2005.

[36] D. Forchetti, G. Garcia, M. I. Valla, "Adaptive Observer for Sensorless Control of Stand-Alone Doubly Fed Induction Generator," *IEEE Trans. on Ind. Electronics*, Vol. 56, N° 10, pp. 4174 – 4180, Oct. 2009.

[37] Ngoc-Tung Nguyen, Hong-Hee Lee, "An effective harmonic elimination for DFIG feeding non-linear loads in stand-alone operation ", *38th Annual conference on IEEE Ind. Electron. Soc. IECON 2012*, Oct. 2012, pp. 3527-3532.

[38] A. Di Gerlando, G. Foglia, M. F. Iacchetti, R. Perini, "Analysis and Test of Diode Rectifiers Solutions in Grid Connected Wind Energy Conversion Systems Employing Modular Permanent Magnet Synchronous Generators ", *IEEE Transactions on Industrial Electronics*, vol. 59, no. 5, May 2012, pp. 2135-2146.